An XPS and thermogravimetric study of oxidized AlN and AlN–Si_3N_4 layers deposited by liquid-phase chemical vapour deposition

R. PERREM, F. HENRY, G. PERAUDEAU, B. ARMAS, R. BERJOAN
Institut de Science et génie des Materiaux et Procédés, BP5 Odeillo, 66125 Font Romeu cedex, France

E. BÊCHE
LERMPS, IPSé, 90010 Belfort cedex, France

The results of a comparative study of the resistance to oxidation of AlN and a codeposit of AlN–Si_3N_4 are presented. The oxidation of both types of layer was performed at 1200 °C in an oxygen gas flow ($p_{O_2} \sim 1$ atm). A thermogravimetric analysis was made, recording the weight gain throughout the oxidation process, and revealed a dramatic improvement in the resistance to oxidation of the codeposit layer when compared with the aluminium nitride layer. An X-ray photoelectron spectroscopy depth-profile analysis was made by performing a series of successive abrasive polishes on the oxidized layers. After each abrasive polish the sample surface was cleaned by ionic bombardment under ultrahigh vacuum and the photoemission spectra recorded. This process of polishing, etching and analysis was continued until the oxygen content decreased to a level comparable with that observed in the layers before oxidation. The changes in chemical bonding throughout the various depth profiles were examined by deconvolution of the Al 2p and Si 2p photoelectron peaks and by analysis of the Auger *K L L* lines. It was concluded that the slower rate of oxidation of the codeposit could be attributed to either the formation of silica or a mixed oxide phase of the mullite type (3 Al_2O_3–2 SiO_2).

1. Introduction

In the past both aluminium and silicon nitrides have presented great potential as ceramic materials for high temperature and microelectronic applications [1, 2]. In recent years there has been an ever increasing demand for high-temperature protective coatings using ceramics and refractory materials which are generally found to exhibit high chemical resistance and good thermomechanical properties. A large number of studies have been made of both aluminium and silicon nitrides to investigate their various properties and applications [3–6]. However, there has been little study, to date, of the mixed Al–Si–N system. The current work was therefore undertaken because of the previous lack of study of this particular area and the general interest in recent years for the production of high-performance ceramics. Furthermore, it was hoped that by producing a co-deposit of AlN and Si_3N_4, a new material might be achieved with greater oxidation resistance than either of its component nitrides.

Here, we present the results of a depth-profile analysis which was made using X-ray photoelectron spectroscopy (XPS) measurements. The chemical composition of the Al–Si–N layer was calculated by quantification of the photoelectron peaks observed using the appropriate Scofield atomic sensitivity factors [7] which were corrected by analysis of similarly prepared reference samples. The changes in chemical bonding throughout the depth profile were examined by deconvolution of the Al 2p and Si 2p peak features, and by analysis of the Auger *K L L* lines excited by high-energy bremsstrahlung radiation emitted by the Al K_α X-ray source. The modified Auger parameters were calculated using the energy difference between the 2p photoelectron lines and the Auger *K L L* lines. The value of the Auger parameter is characteristic of a particular chemical bond type and is particularly useful for samples such as those analysed in this study, which exhibit shifts due to charging effects of up to 6 eV, because it is independent of charging effects. The results of a thermogravimetric analysis of the oxidation of both AlN and AlN–Si_3N_4 are discussed in the light of previous studies made by various authors. Finally, on the basis of the XPS depth-profile analysis, reasons for the superior resistance of the codeposit to oxidation are suggested.

0022–2461

2. Experimental procedure

2.1. Preparation of AlN layers

The experimental system used was a vertical hot-wall reactor composed of a graphite susceptor heated using an r.f. induction coil. First, a layer of SiC was deposited on graphite samples of 10 mm diameter and 2 mm thickness. The SiC layer was formed by pyrolysis of tetramethylsilane (TMS) in the presence of hydrogen. The deposition conditions which allow the deposition of pure silicon carbide have been previously reported [8]. Once the SiC layer had been deposited, the H_2/TMS flow was stopped and nitrogen gas injected into the chamber until the temperature in the reaction chamber was lowered to 1150 °C. When the temperature in the reaction chamber became stable, the AlN layer deposition was begun. The AlN layer was produced by pyrolysis of $AlCl_3$ and NH_3 gas mixtures, which were used as the precursors. The $AlCl_3$ gas in this case was produced by passing silicon tetrachloride gas through an aluminium charge maintained at a temperature of 520 °C and a pressure of 200 torr (1 torr = 133.322 Pa) maintained by introduction of nitrogen carrier gas flow.

At a temperature of 520 °C, the gaseous aluminium trichloride was produced by the following reaction,

$$4Al(s) + 3\ SiCl_4 \rightarrow 4\ AlCl_3(g) \qquad (1)$$

The aluminium trichloride and ammonia precursors were injected through separate gas flow lines whose flow rate was controlled using mass-flow controllers, to avoid reaction outside the chamber. The deposition conditions were: $D_{NH_3}/D_{AlCl_3} = 1$; $D_{N_2}/D_{AlCl_3} = 400$; $P = 200$ Pa; $T = 1150$ °C. Using these conditions, crystalline deposits of AlN were formed with an estimated thickness of 30 μm, according to thermogravimetric measurements.

2.2. Codeposit preparation

The codeposit samples were produced under the same sample preparation conditions as the aluminium nitride layers with the exception that silicon tetrachloride and the $AlCl_3$ gaseous precursors were injected through separate gas lines to avoid reaction outside the reaction chamber. The codeposit was thus produced by pyrolysis of both aluminium trichloride and silicon tetrachloride with the composition controlled as a function of the ratio of these two precursors. The deposition conditions were: $D_{NH_3}/D_{AlCl_3} = 4$; $D_{N_2}/D_{NH_3} = 100$; $P = 200$ Pa; $T = 1150$ °C. Using these deposition conditions, the codeposit layers obtained were found to contain a mixture of nanocrystallized AlN dispersed in an amorphous silicon nitride matrix. The microstructure was confirmed using high-resolution transmission electron microscopy (HRTEM) measurements [9].

2.3. Thermogravimetric analysis (TGA)

The TGA technique monitors the changes in sample weight as a function of time and temperature under controlled atmospheres. The weight change can be related to the reaction kinetics or the sample decomposition, and usually correlated with other physical and chemical parameters. The weight change during oxidation of both AlN and AlN–Si_3N_4 samples was monitored using a SETARAM MTB 10^{-8} microthermobalance coupled with a symmetric tungsten oven. In order to avoid system errors, a symmetric system was used with both the sample and reference alumina support suspended in parallel identical tubes inside the oven, giving a sensitivity of ± 0.1 μg.

2.4. XPS analysis

The XPS analysis was performed using an SIA 200 Riber Cameca UHV device. The photoelectron emission spectra were obtained using an AlK_α X-ray source ($h\nu = 1486.6$ eV) striking the surface of the sample. The high-energy bremsstrahlung radiation emitted by the AlK_α X-ray source allowed observation of the high-energy Al *K L L* and Si *K L L* Auger lines. The kinetic energy of both the photoelectron and Auger electrons was measured using a Riber Cameca MAC 2 spectroscopic two-stage analyser. The analyser resolution was fixed at 1 eV. A Riber Cameca CI 50 Ar^+ ion gun (4 keV ion energy) with its associated differential pumping system, was used to remove adsorbed surface contaminants. The insulating properties of these deposits produced surface charging effects, resulting in electron lines being shifted to lower kinetic energies. The peak positions were calibrated with respect to the position of C 1s carbon contamination peak usually located at about 285 eV [10], when observed without charging effects. The chemical composition after abrasive polishing and ionic cleaning of the surface was made by quantification of the corresponding photoelectron peaks.

It should also be noted that the codeposit sample used in the spectroscopic study was the same as that discussed in the thermogravimetric analysis. However, because the oxidation kinetics of AlN are much faster than the codeposit, the AlN sample used for spectroscopic analysis was oxidized for only 5 min at 1200 °C in an oxygen flow in order to produce an oxide layer of comparable thickness.

3. Results of thermogravimetric study and XPS depth profile analysis of oxidized AlN and codeposit layers

3.1. Thermogravimetric results.

Fig. 1 shows the plot of oxide layer thickness versus oxidation time, clearly showing that the codeposit exhibits enhanced resistance against oxidation, forming less than 0.3 μm after heating at 1200 °C for 300 min in an oxygen flow. It has been established that for temperatures above 1200 °C, the oxidation of AlN is governed by a parabolic rate law, indicating a diffusion-limited process. In the initial stages of oxidation of the codeposit, the oxidation curve quickly reaches an asymptotic limit suggesting that the oxide layer formed is almost impermeable to oxygen diffusion in the temperature range measured. It is thought that the slower rate of oxygen diffusion may be caused by

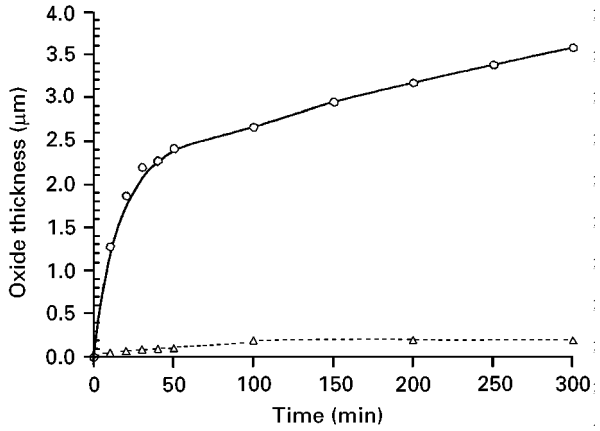

Figure 1 Plot of oxide layer thickness versus oxidation time for (– ○ –) AlN and (– – △ – –) codeposit samples heated at 1200 °C for 300 min.

either the formation of a silica matrix or a mullite-type phase ($3Al_2O_3$–$2SiO_2$).

It should be noted that the thickness of the oxide layers formed at the surface were estimated supposing that the oxide layer was composed of alumina in the case AlN, and alumina and silica in the case of the codeposit. Thus the layer thicknesses were calculated using the theoretical density values for bulk Al_2O_3 and bulk SiO_2 without taking into consideration the variations due to porosity and other morphological defects.

The weight gain of both the AlN and codeposit samples during the oxidation process was used to estimate the thickness of oxide layers formed on the surface. Consequently, the values shown in Fig. 1 must be taken as approximate values, given that it is very likely the oxide layer will exhibit some degree of porosity. Furthermore, it is possible that the oxidized zone itself is not homogeneous and may consist of a mixture of oxide and nitride grains and not a pure oxide layer formed on a pure nitride phase. Such a mixture of phases would also introduce errors in the thickness estimations.

Therefore, it may be concluded that the oxide layer thickness calculations were subject to a significant degree of error and should not be considered absolute values. Nevertheless, even at a qualitative level, the thermogravimetric results clearly show that oxidation kinetics of the codeposit. AlN–Si_3N_4 are much slower than those of the pure AlN layer.

3.2. XPS depth profile analysis results

3.2.1. Oxidized AlN layers

Spectra A–D shown in Fig. 2 are typical XPS survey scans of a depth-profile analysis of an AlN layer after oxidation at 1200 °C for 5 min. Spectra A and B were recorded both before and after 40 min defocalized ionic bombardment of the oxidized AlN surface. These spectra exhibit photoelectron peaks for the following transitions: O 1s, C 1s, Al 2s and Al 2p. The surface spectrum labelled A recorded before ionic bombardment, is indicative of an alumina surface contaminated by adventitious carbon. Spectrum B,

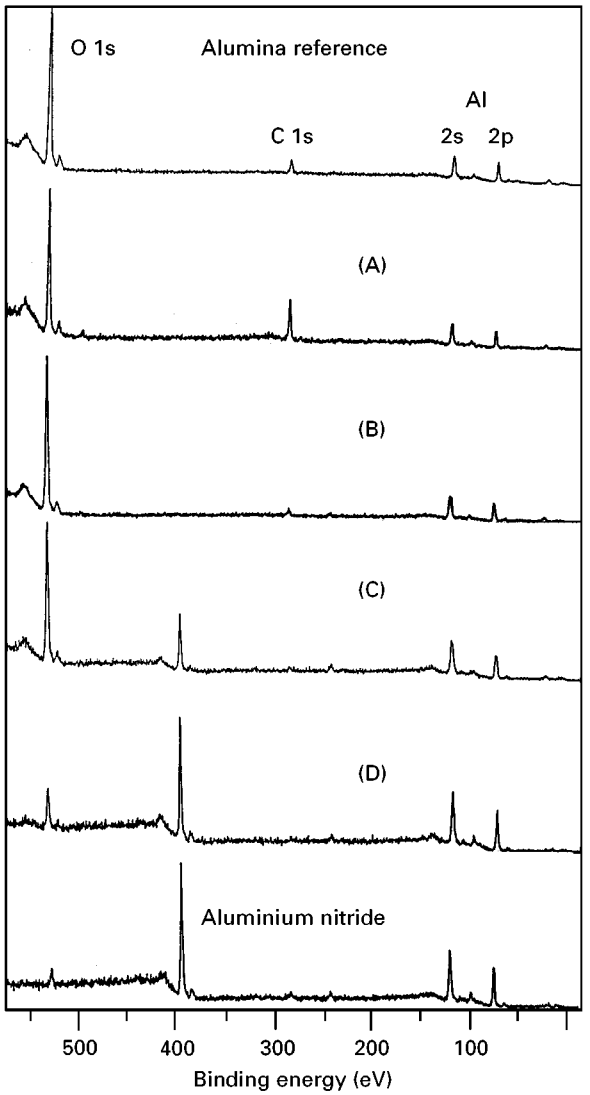

Figure 2 XPS survey scans of AlN and Al_2O_3 reference samples and depth profile spectra A–D of the oxidized AlN layer. A, oxidized surface; B, sputtered oxidized surface; C, 3 abrasive polishings; D, 6 abrasive polishings.

recorded after ionic bombardment of the surface reveals a characteristic spectrum essentially the same as the alumina reference spectra. The XPS survey scans C and D, which were recorded after three and six abrasive polishings, respectively, and ionic etching of the surface show the appearance of the N 1s photoelectron peak, indicating that the aluminium nitride phase has been reached. Spectrum D is in good agreement with the aluminium nitride reference spectrum shown, but shows a greater quantity of oxygen remaining, which is thought to be incorporated into the film matrix during the film growth stages and not as a result of post-deposition oxidation . Therefore, the XPS survey scans suggest a predominance by aluminium oxide in the surface and sub-surface regions. Further abrasive polishing reveals an intermediary region which could be indicative of an oxynitride phase and, finally, after six abrasive polishes, the oxide layer is effectively traversed and the resulting surface spectrum indicative of aluminium nitride with small traces of oxide phases remaining.

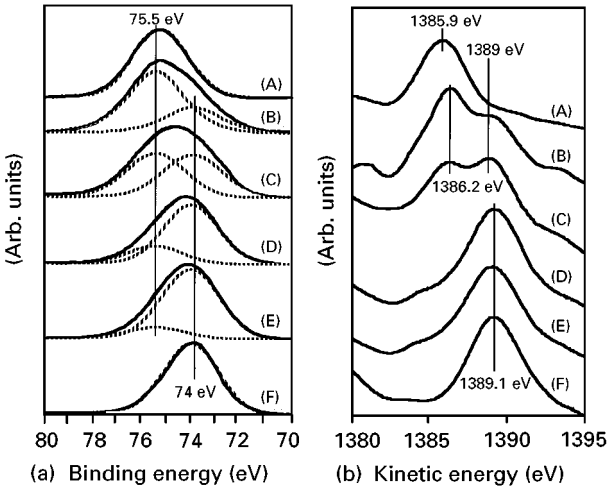

Figure 3(*a*) Al 2p and (b) Al *K L L* line-shapes collected on the oxidized AlN deposit. Spectra A–F were recorded after 1–6 abrasive polishings of 5 min duration.

Fig. 3a and b show a more detailed depth-profile analysis illustrating the evolution of the Al 2p photoelectron peak and the corresponding Auger *K L L* line recorded after a series of successive abrasive polishes of the oxidized AlN surface. It should also be noted that all spectra were recorded after defocalized ion etching of the surface to remove surface contaminants. Spectra A–F shown in Fig. 3 were recorded after one to six abrasive polishings of 5 min duration, respectively.

The Al 2p peak deconvolution was made using Gaussian components with a full-width at half-maximum (FWHM) of approximately 2.6 ± 0.1 eV. The FWHM values used were estimated from similarly prepared reference samples. The estimated FWHM values are slightly higher than are usually quoted for materials of this type [11] owing to the highly insulating nature of the samples, surface morphology [12], and the presence of amorphous phases [9]. The photoelectron peak evolution shown in Fig. 3a suggests a transition from a surface dominated by Al–O bonding, with a single component located at 75.5 eV, to the original nitride phase indicated by a single component located at 74 eV [10]. The peak deconvolutions revealed a simple decrease in the oxide contribution paralleled by an increase in the nitride-phase contribution as the oxidized region was traversed through spectra A–F. Fig. 3b shows the same peak evolution as that shown in Fig. 3a but for the Auger *K L L* transition. It may be seen that there are also two major contributions in the series of spectra, corresponding to oxide and nitride phases observed at 1386.1 and 1389.1 eV, respectively. The peak separation between the two *K L L* peaks for the oxide and nitride phases of aluminium is approximately 3 eV, which is twice the peak shift observed in the corresponding Al 2p peak deconvolution. The first three Auger *K L L* spectra recorded after 1, 2 and 3 abrasive polishings, exhibit significant contributions for both oxide and nitride phases. Spectra D–F recorded after 4, 5 and 6 abrasive polishings, show a predominance of the AlN contribution located at 1389.1 eV.

Table I lists the spectral data calculated using the photoemission spectra shown in Fig. 3. It may be seen from the estimated atomic percentages that the same trend as shown in the aluminium peak evolutions is observed with a decrease in oxide content paralleled by an increase in the nitride phase contribution throughout the depth profile. The modified Auger parameter values are in good agreement with the reference sample values quoted in Table II and with those values normally quoted for oxide and nitride phases of aluminium [13, 14]. However, the Al 2p peak positions for the oxide component is somewhat higher than that quoted for bulk Al_2O_3 [15].

It may therefore be concluded that the photoelectron and Auger *K L L* peak evolutions reveal that at 1200 °C, oxidation of AlN in air occurs by a direct mechanism, without the formation of intermediary oxynitride phases. This conclusion is in agreement with the results of previous studies by Labatut *et al.* [16] and Azema *et al.* [17] who observed that at temperatures above 1000 °C, oxidation of AlN leads to direct formation of α-Al_2O_3.

Furthermore, it should be noted that there were no substoichiometric phase or structural defect contributions, often observed in depth profiles of this type. This observation is in agreement with the results of several recent studies [18–20] which have concluded that aluminium oxide does not suffer from preferential sputtering or reduction during argon ion bombardment.

TABLE I Spectral data for the XPS depth profile of an oxidized AlN layer recorded after 1–6 abrasive polishings of 5 min duration with all spectra recorded after ionic bombardment

Polishing number	Composition ($\pm$ 3 at %)				Binding energy ($\pm$ 0.3 eV)				Modified Auger parameter, α' ($\pm$ 0.3 eV)
	O(%)	N(%)	C(%)	Al(%)	O 1s	N 1s	C 1s	Al 2p	
1	53	0	7	40	532.1	–	284.9	75.6	1461.7
2	41	17	5	37	532.2	396.8	284.8	75.5	1461.7 1463
3	36	22	3	43	532.4	396.9	285	74.7	1461.7 1463
4	18	34	3	45	532.3	397	285	74.3	1463.1
5	13	36	7	44	532.2	396.9	285	74.1	1463.1
6	7	45	0	48	532.3	397.1	—	74	1463.1

TABLE II Spectral data for reference samples of alumina and aluminium nitride

Composition (± 3 at %)				Binding energy (± 0.3 eV)				E_K Al *K L L* (eV) (± 0.3 eV)	Modified Auger parameter α' (± 0.3 eV)
O(%)	N(%)	C(%)	Al(%)	O 1s	N 1s	C 1s	Al 2p		
Aluminium oxide									
52	–	13	34	533	–	285	75.3	1386.2	1461.9
Aluminium nitride									
3	47	7	42	532.7	497.3	284.9	74	1389.1	1462.9

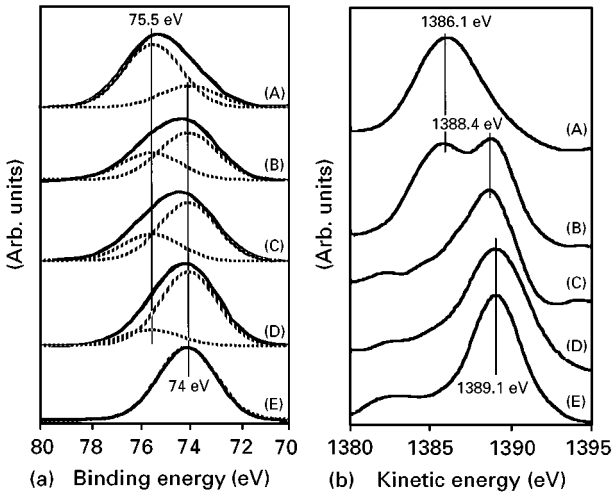

Figure 4(*a*) Al 2p and (b) Al *K L L* line shapes collected on the oxidized AlN–Si_3N_4 codeposit. Spectra A–E were recorded, respectively, after 1,4,5,6 and 7 abrasive polishings of 5 min duration.

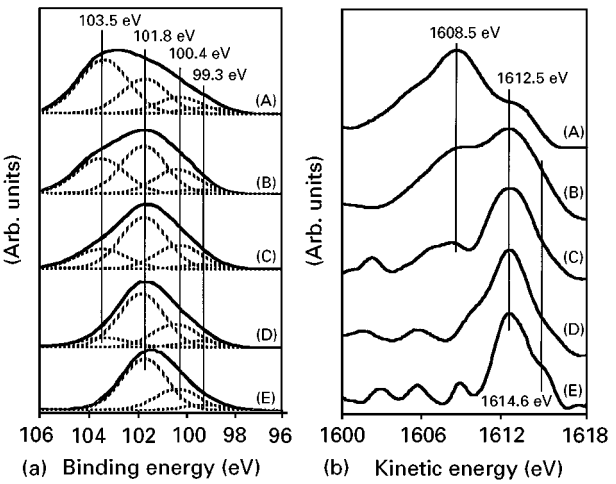

Figure 5(*a*) Si 2p and (b) Si *K L L* line shapes collected on the oxidized AlN–Si_3N_4 codeposit. Spectra A–E recorded, respectively, after 1,4,5,6 and 7 abrasive polishings of 5 min duration.

3.2.2. Oxidized codeposit layer

Fig. 4a shows a similar Al 2p photoelectron peak depth profile as that shown in Fig. 3a, but for aluminium, in the codeposit film oxidized for 300 min at 1200 °C in air. Spectra A–E were recorded, respectively, after 1,4,5,6, and 7 abrasive polishes of 5 min duration and after ionic cleaning to remove surface contamination. The peak deconvolution made was similar to that used in Fig. 3b, with Gaussian components of FWHM values 2.6 ± 0.1 eV. The Al 2p peak evolution for the codeposit exhibited two components located at 74 and 75.5 eV which are indicative of Al–N and Al–O bonding, respectively. The depth-profile analysis showed that after a series of successive abrasive polishes, the Al 2p oxide component decreases and the nitride contribution increases. Fig. 4b shows the Auger *K L L* spectra recorded after the same series of abrasive polishes as discussed in Fig. 4a and exhibits three significant peaks observed at 1386.1, 1388.4 and 1389.1 eV. The first and last of these three peaks may be attributed to Al–O and Al–N bonding, respectively. The broad peak observed in spectra (B) and (C) at 1388.4 eV is thought to be simply the sum of oxide and nitride contributions, rather than an indication of an actual oxynitride intermediary phase. As discussed earlier, the results of a number of previous studies [16, 17] indicate that at temperatures above 1000 °C, AlN oxidizes directly to form α-Al_2O_3 which suggests the formation of an oxynitride intermediary is unlikely. Therefore, it was concluded that the oxidation of AlN in the codeposit proceeds by the same mechanism as in the pure AlN layer. This conclusion is also in agreement with the results of a theoretical study by Weitzer *et al.*. [21] who suggested that no ternary phase was present in the solid solution of the Al–Si–N system.

Fig. 5a shows the Si 2p peak evolution in the oxidized codeposit layer, with spectra A–E again recorded, respectively, after 1,2,4,5,6,7 abrasive polishes and ionic cleaning of the surface. The silicon photoelectron peak evolution revealed generally broader peaks, indicative of a more complex mixture of phases and bonding structures than observed in the corresponding aluminium photoelectron peaks. It should be noted that the peak-fitting deconvolution was made using Gaussian components with FWHM values between 2.1 and 2.4 eV. There were four peak contributions observed at 103.5, 101.8, and 100.4 and 99.3 eV. The components seen at 103.5 and 101.8 eV may be attributed to silicon tetrahedrally bonded with oxygen (SiO_4) [22] and nitrogen (Si_3N_4) [23, 24]. Other significant contributions were observed at ~100.4 and 99.3 eV and may be, respectively, attributed to a substoichiometric phase of the type SiN_x [25], and the presence of Si–Si_4 tetrahedra, dangling bonds and other structural defects [26]. A number of previous studies have cited the tendency for preferential sputtering of nitrogen from nitrides leading to the

TABLE III Spectral data for the XPS depth profile of the codeposit layer oxidized at 1200 °C, recorded after 1,4,5,6 and 7 abrasive polishings of 5 min duration with all spectra recorded after ionic bombardment

Polishing number	Composition ($\pm$ 3 at %)					Binding energy ($\pm$ 0.3 eV)		Modified Auger parameter, α' ($\pm$ 0.3 eV)	
	O(%)	N(%)	C(%)	Si(%)	Al(%)	Si 2p	Al 2p	Si	Al
1	54	5	9	9	27	103.0	75.2	1711.7	1461.6
4	32	23	5	13	27	101.8	74.3		1461.6 1462.4
5	19	33	3	13	29	101.7	74.3	1714.2	
6	12	38	4	14	32	101.7	74.1	1714.2	1463.1
7	6	47	0	11	36	101.5	74	1713.8	1463.1

formation of structural defects and deviations from stoichiometry [25, 26]. The substoichiometric SiN_x phase contribution to the Si 2p peak deconvolution varies between 14% and 26% of the total peak area thoughout the depth profile. It has been reported that liquid-phase chemical vapour deposition (LPCVD) nitride layers usually contain $\sim 5\%$ silicon in the subnitride state which rises to 10–15% upon ion bombardment of the sample surface [27]. Therefore, it is thought probable that the majority of the deviation from stoichiometry and structural defect contributions to the Si 2p peak spectra are caused by ionic bombardment of the surface. However, it is also suggested that the remainder, 5%–10% of the subnitride contribution is caused by local atomic rearrangements occurring during the oxidation process.

Fig. 5b shows the Auger Si KLL depth profile spectra A–E for the oxidized codeposit recorded, respectively, after 1,4,5,6 and 7 abrasive polishes and subjected to ionic bombardment after each polish. The principal peak contributions in this spectra are observed at 1608.5, 1612.5 and 1614.6 eV, which may be attributed to Si–O, Si–N, and Si–Si bonding, respectively [28]. After each successive polish, a progressive decrease in the oxide bonding contribution is observed paralleled by an increase in the corresponding Si–N bonding contribution. The Si–Si covalent peak is observed as a high-energy shoulder on the silicon nitride peak located at 1614.6 eV.

Table III summarizes the compositions and the experimental Si 2p and Al 2p peak position measured for the oxidized codeposit layer from the XPS spectra collected on samples A–E after the same series of successive abrasive polishes as discussed in Fig. 4a, b, 5a and b. The calculated modified Auger parameters are also reported in Table III. The Si 2p peaks located at 103 ± 0.3 and 101.7 ± 0.3 eV are characteristic of, respectively, $Si(O)_4$ and $Si(N)_4$ chemical bonds. The Al 2p peaks located at 75.2 ± 0.3 and 74.2 ± 0.3 eV are attributed, respectively, to Al_2O_3 and AlN compounds. The modified Auger parameter values were calculated using the energy difference between the Auger KLL peak positions and the corresponding deconvoluted component of the photoelectron peak. The Auger parameter values calculated for silicon, 1711.7 ± 0.3 and 1714.2 ± 0.3 eV, were attributed, respectively, to $Si(O)_4$ chemical bonds in SiO_2 and $Si(N)_4$ chemical bonds in Si_3N_4 [10]. Those for aluminium 1461.6 ± 0.3 and 1463.1 ± 0.3 eV, were attributed, respectively, to Al–O chemical bonds in Al_2O_3 and Al–N chemical bonds in aluminium nitride [10]. It is notable that only one value of the Auger parameter α', calculated from the spectrum collected after four abrasive polishes for aluminium ($\alpha' = 1462.4 \pm 0.3$ eV) could not be attributed to Al–N chemical bonds. This value of α' may result from the overlapping of two Si KLL peaks due to Si–O and Si–N bonds. From the results reported in Figs 4 and 5 and in Table III, we can conclude that the thickness of the oxidized layer formed on the codeposit Si_3N_4–AlN surface after an oxidation duration of 300 min at 1200 °C was similar to the thickness of the oxidized layer formed on the pure AlN deposit after 5 min oxidation. Indeed, 6 or 7 identical polishings were necessary to reach the bulk of the AlN and AlN–Si_3N_4 deposit.

4. Discussion

4.1. AlN oxidation

In both the AlN and codeposit depth profiles, peak shifts between oxide and nitride phases of aluminium of approximately 1.5 eV for the photoelectron peak and ~ 3 eV for the Auger KLL line were consistently observed. A number of authors have discussed the difficulties of differentiating between oxide and nitride phases of aluminium using Al 2p and Al KLL lines. Katnani and Papothomas [29] found that the main obstacle to identification of aluminium oxide commonly present on the surface of bulk aluminium nitrides was the near equivalence of the Al 2p binding energies for the two phases. More recent studies by Liao *et al.* [14] and Wang *et al.* [30] concluded that the Al KLL peak shift was sufficient to allow identification of oxide and nitride phases, observing peak separations of 2.2 and 2.4 eV, respectively.

The Al 2p photoelectron peak positions for oxide bonding have, in the past, been the subject of certain controversy due to the large range of values generally reported for certain oxides [31] and, in particular, the Al 2p peak for aluminium oxide [32–35]. However, in the current study, the Al 2p and Al KLL shifts between oxide and nitride phases of aluminium were sufficient to allow identification of these compounds. Calculations of the modified Auger parameter values

allowed us to confirm the presence of Al–O and/or Al–N chemical bonds. The Auger parameter values are generally unaffected by Fermi level variations and charging effects. The modified Auger parameter values calculated for aluminium in both the AlN layer and codeposit correspond closely to literature values normally quoted for oxide and nitride phases of aluminium [13, 14]. Thus, our XPS results show that the direct formation of Al_2O_3 is highly probable during the oxidation of AlN at 1200 °C under an oxygen pressure of 1 atm.

4.2. Si_3N_4 oxidation

It was also thought necessary to investigate the possibility of intermediary oxynitride phase formation for silicon in the codeposit. The absolute values for both Si 2p and Si *K L L* peak positions which have been previously attributed to silicon oxynitride phases, lies between those values quoted for SiO_2 and Si_3N_4 phases [36]. The results of two recent studies [37, 38] show that the Si *K L L* peak position for oxynitride layers varies linearly as a function of oxygen to nitrogen ratio, between 1608 eV for SiO_2 and about 1612 eV for Si_3N_4. A similar correlation was observed by Lozzi *et al.* [38] for the modified Auger parameter values varying between $\sim$1711.5 eV for SiO_2 and about 1714 eV for Si_3N_4. Such evolution of the Si *K L L* peak positions or modified Auger parameter values were not clearly observed in this work. It is particularly obvious that the Si *K L L* line shapes shown for samples A–C in Fig. 5b are characteristic of Si_3N_4 and SiO_2 mixtures whereas the Si *K L L* line shapes for samples D and E show a clear predominance of silicon nitride. Thus, it was concluded that the presence of an intermediary SiO_xN_y phase in the oxidized codeposit layer was not detected in this work. However, the formation of such an intermediary phase as a minor constituent in the oxidized layer remains possible.

5. Conclusions

It may be concluded that in traversing the oxidized region of the codeposit, a simultaneous increase in the concentration of Al–N and Si–N bonding contributions is observed at the expense of Al_2O_3 and SiO_2 type bonding. It may be further deduced that in the case of the codeposit there is no preferential oxidation of one of the nitride phases present over the other. However, it may be seen that the oxidation of pure aluminium nitride progresses far more quickly than the codeposit.

Transmission electron microscopy measurements have revealed that codeposit samples were composed of a mixture of nanocrystallites of AlN embedded in an amorphous silicon nitride matrix. It is thought that the oxidation of both nanocrystallized AlN and Si_3N_4 (amorphous) phase occurs simultaneously throughout the codeposit depth profile. This simultaneous oxidation indicates that the oxidation of the two phases is controlled by the same processes of oxygen transfer from the surface region to the bulk of the layer.

The slow rate of oxygen diffusion in the codeposit may be attributed to either the formation of silica, or a mixed oxide phase of the mullite type ($3Al_2O_3$–$2SiO_2$), in which the rate of oxygen diffusion would be greatly reduced.

References

1. Y PAULEAU, J. J. HARTZPERGUE and J. C. REMY, *Bull. Soc. Chim. Fr.* **5–6** (1979) 199.
2. F. L. RILEY, *Sci. Ceram.* **12** (1983) 15.
3. M. FEIL, *Hybrid Circuits*, **18** (1989) 29.
4. K. T. McGARRON, G. R. KLINE, J. T. MARTIN and K. M. LARKIN, *IEEE Ultrason. Symp. Proc* **1** (1988) 673.
5. K. ANDO, A. ISHITANI and K. HAMANO, *Appl. Phys. Lett.* **59** (1991) 1083.
6. H. KUROGI, N. INOUE, M. TAKAHASHI, H. TAMURA, T. AJIOKA, M. YOSHIMARU and M. INO, IEICE Tech Rep SDM91-30 (1991) p. 43.
7. J. H. SCOFIELD, *J. Electron Spectrosc.* **8** (1976) 129.
8. B. ASPAR, R. BERJOAN, C. LABATUT and B. ARMAS, *Appl. Surf. Sci.* **81** (1994) 55.
9. FRANK HENRY, PhD thesis, Université de Montpellier, January 1995.
10. D. BRIGGS and M. P. SEAH, "Practical Surface Analysis by Auger and X-ray Photoelectron Spectroscopy" (Wiley, Chichester, 1983) p. 363.
11. Ch. GRUNDLING, J. ALERCHER and D. W. GOODMAN, *Surf. Sci.* **318** (1994) 97.
12. F. HENRY, B. ARMAS, M. BALAT, R. BERJOAN and C. COMBESCURE, *J. Phys. IV*, *Coll. C3*, *Suppl. J. Phys.* **23** (1993) 519.
13. J. A. TAYLOR and J. W. RABLAIS, *J. Chem. Phys.* **75** (1981) 1735.
14. H. M. LIAO, R. N. S. SODHI and T. W. COYLE, *J. Vac. Sci. Technol.* **A11** (1993) 2681.
15. C. P. WAGNER, W. M. RIGGS, L. E. DAVIS, J. F. MOULDER and G. E. MUILENBERG, "Handbook of X-ray Photoelectron Spectroscopy" (Perkin-Elmer, Eden, Prairie, MN, 1979).
16. C. LABATUT, D. KHARCHI, B. ASPAR, F. SIBIEUDE and B. ARMAS, *J. Eur. Ceram. Soc.* **13** (1994) 339.
17. N. AZEMA, J. DURAND, R. BERJOAN, C. DUPUY and C. LOT, *ibid.* **8** (1991) 291.
18. V. ANDRE, F. AREFI, J. AMOUROUX and G. LORANG, *Surf. Interface Anal.* **16** (1990) 241.
19. M. P. SEAH, *Vacuum* **34** (1984) 463.
20. S. HOFFMAN, *J. Trace Microprobe Technol.* **1** (1982/83) 213.
21. F. WEITZER, K. REMSCHNIG, J. C. SCHUSTER and P. ROGL, *J. Mater. Res.* **8** (1990) 2152.
22. E. BECHE, R. BERJOAN, J. VIARD, B. CROS and J. DURAND, *Thin Solid Films* **258** (1995) 143.
23. C. D. WAGNER, *Surf. Interface Anal.* **12** (1988) 527.
24. S. I. RAIDER, R. FLITSCH, J. A. ABOAF and W. A. PLISKIN, *J. Electrochem Soc* **123** (1976) 560.
25. M. KAZUTA, N. SO, H. KASAMURA and M. KUDO, *Surf. Interface Anal.* **19** (1992) 222.
26. H. BENDER and W. D. CHEN, *ibid.* **15** (1990) 38.
27. F. PAVLYÀK, I. BERTOTI, M. MOHAI, I. BUZCO and J. GIBER, *ibid.* **20** (1993) 221.
28. J. A. TAYLOR, *Appl. Surf. Sci.* **7** (1981) 168.
29. A. D. KATNANI and K. I. PAPOTHOMAS, *J. Vac. Sci. Technol.* **A5** (1987) 1335.
30. P. S. WANG, S. G. MALGHAN and S. M. HSU, *J. Mater. Res.* **10** (1995) 302.
31. W. F. EGELLHOFF, *J. Surf. Sci. Rep.* **6** (1987) 253.
32. T. L. BARR, S. SEAL, L. M. CHEN and C. C. KAO, *Thin Solid Films* **253** (1994) 277.
33. N. CABRERA and N. F. MOTT, *Rep. Prog. Phys.* **12** (1948) 163.
34. M. CASAMASSIMA and E. DARGUE-CERETTI, *J. Mater. Sci.* **28** (1993) 3997.

35. W. MULLINS and B. L. AVERBACH, *Surf. Sci.* **206** (1988) 41.
36. C. D. WAGNER, D. E. PASSOJA, H. F. HILLERY, T. G. KINISKY, H. A. SIX, W. T. JANSEN and J. A. TAYLOR, *J. Vac. Sci. Technol.* **21** (1982) 933.
37. M. S. HEDGE, R. CARACCIOLO, K. S. HALTON and J. B. WATCHMAN, *Appl. Surf. Sci.* **37** (1989) 16.
38. L. LOZZI, M. PASSACANTANDO, P. PICOZZI, S. SANTUCCI, G. TOMASSI, R. ALFONSETTI and A. BORGHESI, *Surf. Interface Anal.* **22** (1994) 190.

Received 10 August 1995
and accepted 31 July 1996